Shaping and transporting diamagnetic sessile drops

Jennifer Dodoo[1] and Adam A. Stokes[1, a)]
School of Engineering, Institute for Integrated Micro and Nano Systems, The University of Edinburgh, Edinburgh, EH9 3LJ, United Kingdom

Electromagnetic fields are commonly used to control small quantities of fluids in microfluidics and digital microfluidics. Magnetic control techniques are less well studied than their electric counterparts, with only few investigations into liquid diamagnetism. The ratio of magnetic to surface energy (magnetic Bond number B_m) is an order of magnitude smaller for diamagnetic drops ($B_m \approx -0.3$ at 1.2 T applied field) than for paramagnetic drops ($B_m \approx 9.0$ at 1.2 T applied field). This weaker interaction between the magnetic field and the diamagnetic drop has led to the phenomenon being overlooked in digital microfluidics. Our findings highlight how diamagnetic fluids can be used as a novel tool in the toolbox of microfluidics and digital microfluidics.

I. INTRODUCTION

The control of small quantities of fluids is important in microfluidics[1] and digital microfluidics (DMF)[2–4], where drops are manipulated. DMF has strong biomedical applications, such as proteomics, imunoassays, and the study of cells[5–7]. While the electromagnetic control of fluids, particularly for biomedical applications, is dominated by electric phenomena, research into magnetic phenomena is much less common and their capabilities have not been fully realised. Magnetic actuation techniques are highly suitable for biomedical applications, due to the biocompatibility of many magnetic fluids and the possibility to apply large magnetic fields to the human body - as routinely done in Magnetic Resonance Imaging - where contrasting agents contain gadolinium chloride, a paramagnetic salt.

Electromagnetic fields exert forces on ions and electric and magnetic dipoles in the fluid. The potential of controlling fluids with electromagnetic fields has already been recognised in the late 19th century. Important examples include the works on bulk electrowetting by Lippmann[8] - where the interface between a mercury electrode and an electrolyte solution is shaped by an applied voltage; and on bulk dielectrophoresis by Pellat[9] - where the height-of-rise of a column of dielectric liquid (non-volatile oil) is controlled by an alternating (at a frequency of 260 Hz) electric field, as illustrated by Fig. 1a).

Electrowetting-on-dielectric (EWOD) includes a thin layer of dielectric between electrode and liquid to reduce the effects of electrolysis and was first introduced by Berge[10]. EWOD[11–13] and liquid dielectrophoresis[14–17] are common control techniques in DMF, where they are used for drop generation, transportion, splitting and merging[2–7].

Dielectrophoresis of suspended particles (see Fig. 1b)) has found many biomedical applications[18,19], including sorting of cells as demonstrated by Pohl[20].

Liquid magnetophoresis - where fluids containing magnetic dipoles are manipulated by an applied magnetic field - has found wide ranging applications in magnetic DMF[21,22]. Drops of ferrofluids are commonly used in DMF[21–23] and their shape in magnetic fields has been studied extensively[24–26].

An alternative to ferrofluids are solutions of paramagnetic salts - which contain randomly oriented magnetic dipoles. Transportation of paramagnetic drops has first been reported by Egatz-Gomez *et al.*[27] and was studied more recently by Mats *et al.*[28]. We have recently studied the shaping of paramagnetic drops in homogeneous magnetic fields and found an elongation of the drops along the field lines[29], as illustrated by Fig. 1c).

Magnetic fluids that are seldomly studied are diamagnetic liquids ($\chi^m < 0$), such as water or aqueous solutions of diamagnetic salts. A recent review by Bormashenko[30] however highlights the scientific interest and applications of bulk diamagnetism. In particular, recent publications on this topic include work on the magnetic deformation of diamagnetic liquid-air interfaces ('Moses effect')[31] and on floating diamagnetic bodies[32,33]. While these investigations were performed in bulk fluids, to the best of our knowledge, there are no studies on the shaping and control of diamagnetic drops.

In this work, we demonstrate and analyse shaping of a diamagnetic drop in a homogeneous magnetic field. We find a reverse effect to shaping of paramagnetic drops in homogeneous magnetic fields, namely that diamagnetic drops shorten along the direction of the field lines. We also explore the transport of diamagnetic and paramagnetic drops due to magnetic field gradients. The capabilities of diamagnetic fluids have long been overlooked, and investigations into this field provide a wealth of opportunities for scientific studies and applications.

II. THEORETICAL BACKGROUND

The stress on a volume due to electromagnetic fields is captured in the Maxwell stress tensor (MST), which is valid in vacuum. The MST has been used to describe electrohydrodynamic and magnetohydrodynamic phenomena, such as dielectrophoresis[34–36] and electrowetting[35,37], highlighting the frequency-dependence between electrowetting and DEP; and the deformation of ferrofluidic drops in magnetic fields[25,38,39]. The MST is a reduced version of the electromagnetic stress tensor (EMST), which is valid for quasi-static, non-dissipative processes[40]:

$$\sigma_{ik} = (U - TS - \xi_\alpha \rho_\alpha - \mathbf{E}\cdot\mathbf{D} - \mathbf{H}\cdot\mathbf{B})\delta_{ik} + E_i D_k + H_i B_k \qquad (1)$$

where i is the direction of force and k is the direction normal to the surface to which the force is applied, U is the total energy density of matter and field (Jm^{-3}), T is temperature (K),

a)corresponding author: adam.stokes@ed.ac.uk

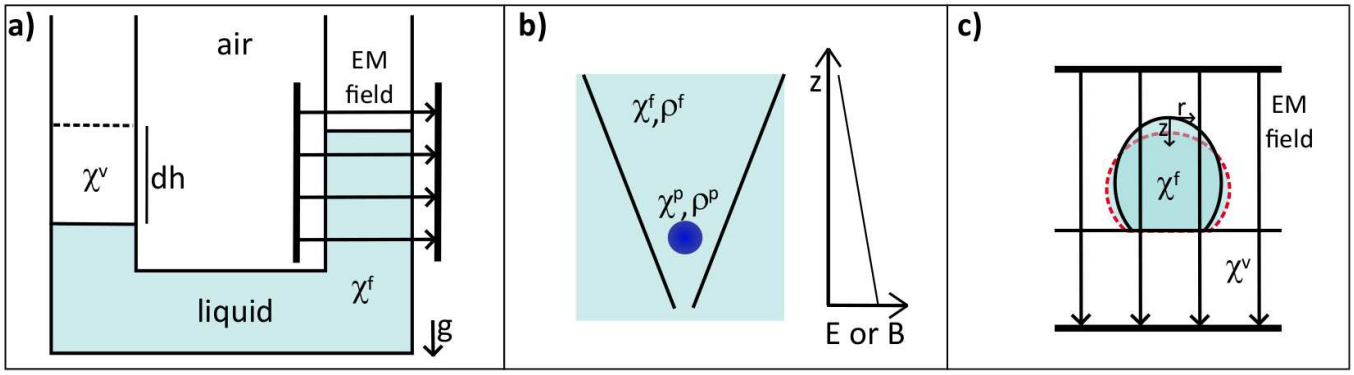

FIG. 1. Illustrations of common electrostatic and magnetostatic fluidic experiments. **a)** The height of a liquid column in air is raised in an electric or magnetic field, where the electric or magnetic susceptibility of the fluid is $\chi^f > 0$, and χ^v is the susceptibility of air. **b)** A particle with magnetic susceptibility χ^p and density ρ^p is suspended in a liquid with χ^f and density ρ^f. In a non-uniform electrostatic or magnetostatic field, the electromagnetic force acting on the particle experiences depends on $\chi^p - \chi^f$. **(c)** A drop of a fluid with χ^f in air with χ^v in a uniform electrostatic or magnetostatic field is elongated for $\chi^f > 0$.

S is the entropy density of matter and field ($\mathrm{Jm^{-3}K^{-1}}$), ξ_α is the mass density of the chemical potential ($\mathrm{Jkg^{-1}}$) of the material component α, ρ_α is the partial density of the material component α (the total density is $\rho^{tot} = \Sigma_\alpha \rho_\alpha$), **E** is the electric field, **D** is the electric displacement field, **H** is the applied (auxiliary) field, **B** is the magnetic flux density, and δ_{ik} is the Kronecker-Delta function.

Using Eq. 1, we have previously shown that in a closed thermodynamic system with thermodynamic potential $a^t = a_0 + a_{em}$, where a_0 and a_{em} are field-indenpendent and field-dependent terms, at constant temperature and volume ($U = a^t + TS$), in the absence of electric fields (**E=D=**0), and with $\xi_\alpha = \delta a^t / \delta \rho_\alpha$, the stress difference across a liquid-air boundary is[29]:

$$\Delta\sigma^M_{nn} = a^l_0 - a^v_0 - \xi_0\rho_\alpha - \frac{1}{2}\mu_0 H^2\left(\chi + \rho_\alpha \frac{\delta\chi}{\delta\rho_\alpha}\right) + \mu_0\chi H_n^2 \qquad (2)$$

The magnetic field is the vector sum of its normal and tangential components with respect to the surface over which $\Delta\sigma^{EM}_{nn}$ is resolved, $H^2 = H_n^2 + H_t^2$.

We can conclude from Eq. 2 that the magnetic stress difference depends on the shape of the interface and its orientation with respect to the applied magnetic field, as well as the magnetic properties of the liquid (χ); the direction of the magnetic stress is independent of the sign of the magnetic field, but is instead determined by the sign of χ; and in a non-uniform magnetic field, the magnitude of $\Delta\sigma^{EM}_{nn}$ varies along the liquid-vapour interface, causing a stronger deformation of the interface in regions of higher magnetic field strength.

To determine the shape of a liquid-vapour interface, the electromagnetic stress needs to be balanced with other stresses such as gravitational and surface stress. Stierstadt and Liu[40] have used the EMST to find an expression for the height-of-rise of a liquid in a magnetic field and for the force on a particle in a fluid. We have previously used the EMST to describe the shape of sessile drops in magnetic fields[29]. The expressions for key parameters of these phenomena are summarised in Table I.

The magnetic stress difference expressed in Eq. 2 can easily be transformed to an electric stress difference[40]:

$$\begin{aligned} \mathbf{H} &\rightarrow \mathbf{E} \\ \mathbf{B} &\rightarrow \mathbf{D} \\ \mu_0 &\rightarrow \varepsilon_0 \\ \chi_m &\rightarrow \chi_e \end{aligned} \qquad (3)$$

This means that the extensive body of work on electrostatic phenomena can be transferred to magnetostatic phenomena with some key differences: charge induced fluid circulations limit the validaty of a static stress balance in dielectrics[44,45] - these circulations are not present in magnetic fluids[46]; natural materials may have a negative magnetic, but not a negative electric susceptibility. These phenomenological differences make the study of magnetostatic phenomena particularly attractive. Here, we exploit the fact that diamagnetic fluids have a negative magnetic susceptibility to demonstrate the reverse effect to the elongation along the field lines of paramagnetic drops in uniform magnetostatic fields[29] and conducting drops in electrostatic fields[47].

III. EXPERIMENTAL DEMONSTRATION: DEFORMATION AND TRANSPORT OF DIAMAGNETIC SESSILE DROPS

To confirm our predictions on the shape of diamagnetic drops from section II, we (1) measure the shape of diamagnetic drops in a homogeneous magnetic field directed along the symmetry axis of the drops (Fig. 1(c)); and (2) demonstrate the transport of diamagnetic drops in a non-uniform magnetic field.

TABLE I. Expressions of key observables of some magnetostatic phenomena in fluids, derived using the electromagnetic stress tensor (Eq. 1)[40].

Phenomenon	Characteristic expression	Label
Change in height (Δh) of a liquid column in air[a]	$\Delta h = \mu_0 \chi_m (2\rho g)^{-1} H_t^2$	(I.1)
Force (**F**) on a particle (p) of volume V_p in a fluid (f)[a]	$\mathbf{F} = \mu_0(\chi_m^p - \chi_m^f) V_p \mathbf{H}\cdot\nabla\mathbf{H}$	(I.2)
Shape of a sessile drop in air[b]	$\gamma(R_1^{-1}+R_2^{-1}) = -g\Delta\rho z + a_0^l - a_0^v - \xi_0\rho_\alpha + \mu_0\chi(H_n^2 - H^2)$	(I.3)

[a] Adapted from Ref.40.

[b] For an axisymmetric drop of a one-component fluid with $\chi << 1$, $\rho(\delta\chi/\delta\rho) = \chi(\chi/3+1) \approx \chi$ and $a_0^l - a_0^v = 2\gamma b^{-1}$, where γ is the surface tension (Nm^{-1}) and b is the radius of curvature at the apex point (m) of the drop[41–43]. We use following definition of the principle radii of curvature, R_1 and R_1, taken from Ref. 42: $(R_1^{-1}+R_2^{-1}) = r''(1+r'^2)^{-3/2} - r(1+r'^2)^{-1/2}$, where r(z) is the drop outline, originating from the apex point, r' and r'' are the first and second derivatives of r with respect to z, and $r(z)$ and r' vanish at the apex point where $z = 0$.

TABLE II. List of properties of the diamagnetic salts and their solutions used in this work.

Solution Name	Salt Formula	M_S g mol^{-1}	χ_m [a] cm^3mol^{-1}	C_S (%ppw)	χ [b]	B_m at B=1.2 T
Calcium bromide	$Br_2Ca\cdot xH_2O$	199.89	-73.8×10^{-6}	55.8	-7.8×10^{-6}	-0.3
Sodium sulphate	$NaSO_4$	142.04	-52×10^{-6}	15.7	-8.3×10^{-6}	-0.3
Manganese chloride	$MnCl_2\cdot4H_2O$	197.9	14350×10^{-6}	27.4	245.0×10^{-6}	8.8

[a] Taken from Ref. 48.

[b] To calculate the magnetic susceptibility of the drop, we use $\chi = \rho(\chi_s^m C_s M_s^{-1} + \chi_w^m(1-C_s)M_w^{-1})$, where M_s and M_w(g mol^{-1}) are the molar masses and χ_s^m (cm^3mol^{-1}) and χ_w^m (cm^3mol^{-1}) are the molar magnetic susceptibilities of the diamagnetic salt and water respectively. C_s is the weight concentration of salt in the solution and ρ is the density of the solution. We assume that the densities of the salt solutions are 1.2, 1.0, and 1.0 times the density of water (990 g l^{-1}) for the $CaBr_2$, $NaSO_4$, and $MnCl_2$ solutions respectively.

A. Experimental Method

For the actuation of the magnetic drops, we use a C-frame adjustable electromagnet containing iron cores with tips of 8 mm diameter. The coils are connected in-series to a programmable power supply (72-2540, Digital-Control and Programmable DC Power Supply 30V 3A, Tenma). The magnetic field is approximately uniform over the width of the core tips, with a ≈ 20 % reduction in field strength over a 10 mm distance to the centre of the core tips at an air-gap of 7 mm. The substrates are microscope glass slides which we coated with superhydrophobic composite films from colloidal graphite[49].

The drops are aqueous solutions of the diamagnetic salts Calcium bromide hydrate ($Br_2Ca\cdot xH_2O$, CAS-No.: 71626-99-8) and sodium sulphate ($NaSO_4$, CAS-No.: 7757-82-6). For the transport measurements we also use the paramagnetic salt manganese chloride tetrahydrate ($MnCl_2\cdot4H_2O$, CAS-No.: 13446-34-9). The salts were sourced from Sigma-Aldrich (Sigma-Aldrich Company Ltd., UK) and their properties are summarized in Table II. The deionized water has a molecular weight of $M_w = 18.02$ g mol^{-1} and a molar magnetic susceptibility of $\chi_w^m = -12.63\times10^{-6}$ cm^3mol^{-1}. To generalize the present study, we define the dimensionless magnetic bond number from the properties of the drop and applied field, which is the ratio of the magnetic to surface energy[50] of the drops:

$$B_m = \frac{\chi B^2 V^{1/3}}{2\mu_0\gamma} \tag{4}$$

The values of B_m for each drop are listed in Table II.

We analyse the shape of the diamagnetic drop using the same methodology as used in Ref. 29 for paramagnetic drops: we image the side-profile of the drop using a digital DSLR-camera and determine the drop outline r(z) using computational image analysis; using a standard least-square method (Levenberg-Marquardt) we iteratively fit the numerically solutions of Eq. (I.3) to the left and right-side of the drop outline independently. To account for the uncertainty in our estimates of the surface tension and density of the drops, we optimize the numerical value of the surface tension for each drop in the absence of magnetic fields. For drops in the presence of magnetic fields, we optimize the value of the field-independent chemical potential, which also accounts for small deviations of a non-axisymmetric drop deformation, caused by inhomogeneties in the roughness of the substrates, manual levelling of the substrate and magnet, and manual positioning of the drop in the centre of the magnetic field. To measure the radius of curvature at the apex point of the drop, we fit a parabolic function to r(z) in the range where Eq. (I.3) vanishes. We measure the left and right contact angle of the drop by fitting second-order polynomials to the section of the outline close to the triple contact line.

We quantify the transport of a drop in a non-uniform magnetic field by measuring the translocation of the projection of the centre-of-mass onto the substrate. We determine the position of the centre-of-mass as the point along the symmetry axis of the drop that splits the drop into two regions with equal volume, assuming the density of the drop is uniform.

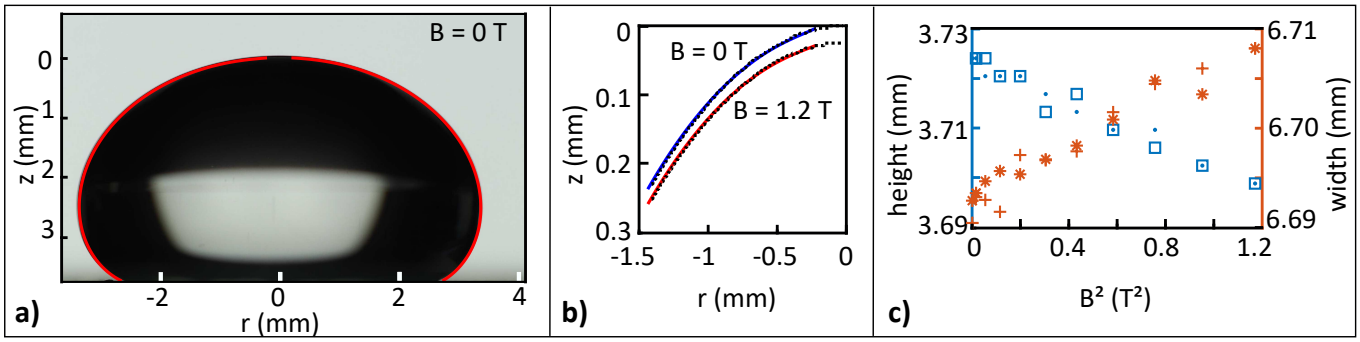

FIG. 2. Deformation of a 100 μl drop of an aqueous solution of calcium bromide (see Table II). (a) The numerical solutions of Eq. (I.3) (blue) is shown on and image of the drop in absence of a magnetic field. (b) Enlarged view of the outline close to the apex point (black, dashed) with the numerical solutions of Eq. (I.3) in the absence of a magnetic field (blue) and with 1.2 T applied field (red). (c) The height decreases (dots) while the width increases (asterisks) with the applied field. As the field is decreased, the height increases (squares) and the width decreases (crosses) to their initial values.

B. Results: shape of a diamagnetic drop

An example of a result of this methodology is shown by Fig. 2. A 100 μl drop of the calcium bromide solution (see Table II) is imaged in the absence of a magnetic field (Fig. 2(a)). The numerical solution of Eq. (I.3) fits well to the outline of the drop. Upon application of a magnetic field, the drop is shortened along the direction of the field lines, as shown by Fig. 2(b), which shows an enlarged view of the outline of the drop at the apex point. The height and width of the drop as a function of applied magnetic field is presented by Fig. 2(c). As the applied field is increased from 0 to 1.2 T, the height reduces from 3.73 to 3.69 mm, and the width increases from 6.69 to 6.71 mm. The change in shape is proportional to the square of the applied field.

We find this deformation to be repeatable, and present the mean and standard error of a measurement set. We find a change in height of (-13 ± 2) μm and (-25 ± 2) μm for 100 μl drops of the calcium bromide and sodium sulphate solutions respectively when changing the applied field from 0 to 0.9 T. The contact angles of the drops in the absence of magnetic fields are $151.6^\circ \pm 1^\circ$ and $151.7^\circ \pm 1^\circ$ for the calcium bromide and sodium sulphate solutions respectively, agreeing with the expected contact angle of water on these substrates[49]. Upon application of 0.9 T, the contact angles of the drops increase to $152.2^\circ \pm 1^\circ$ and $152.2^\circ \pm 1^\circ$ respectively. The numerically optimized parameters of the calcium bromide and sodium sulphate solutions respectively, are the surface tensions (70.7±1) mNm^{-1} and (73.5±1) mNm^{-1}, values which are within two standard errors of the surface tension of water (72.8 mNm^{-1}); and the field-independent chemical potential $(1.8 \pm 1) \times 10^{-4}$ Jkg^{-1} and $(0.7 \pm 1) \times 10^{-4}$ Jkg^{-1}.

These results are in agreement with the predictions made in Section II, namely that drops with a higher magnitude of magnetic susceptibility deform more strongly in a magnetic field; and that a negative susceptibility causes a magnetic stress directed into the liquid phase, leading to a shortening of the drop along the field lines.

C. Results: transport measurements

Example results of the transport measurements of diamagnetic and paramagnetic drops in a non-uniform magnetic field are shown by Fig. 3. The magnetic field decays along the x-axis from a maximum value of B_m as illustrated by Fig. 3(a). A 300 μl drop of the sodium sulphate solution is shown by Fig. 3(b) to lean away from the region of high magnetic flux density, where B_m=0.75 T. Upon increasing B_m the drop is pushed over a distance of approximately 3 mm away from the region of highest magnetic flux density. In contrast to this diamagnetic drop being pushed out of the magnetic field, a drop of 100 μl manganese chloride solution is shown by Fig. 3(c) to lean towards the region of highest magnetic flux density, where B_m=0.4 T. Upon increasing B_m, the drop is pulled over a distance of approximately 12 mm towards the region of highest magnetic field strength.

We found the translocation of the centre-of-mass in these experiments repeatable, with drops of 300 μl sodium sulphate solution pushed over a distance of (3.0±0.3) mm and the drops of 100 μl manganese chloride solutions pulled over a distance of (10.4±0.3) mm.

Consistent with our predictions made in Section II, the transport direction is determined by the sign of χ, while the transport distance is determined by the value χ, the size of the drop, and the field gradient. Due to the field gradient, the drop deforms asymmetrically, causing it to lean into ($\chi > 0$) or out of ($\chi < 0$) the region of higher field strength. The static frictional forces between substrate and drop determine how much the drop leans before sliding.

Our results demonstrate that though the stress acting on diamagnetic drops is several orders of magnitude smaller than on paramagnetic drops, it is nevertheless sufficient to achieve transport even in a simple experimental design as we have employed here. Diamagnetic solutions enable the reversal of transport direction, compared to paramagnetic solutions or ferrofluids, without the need to alter the actuation mechanism.

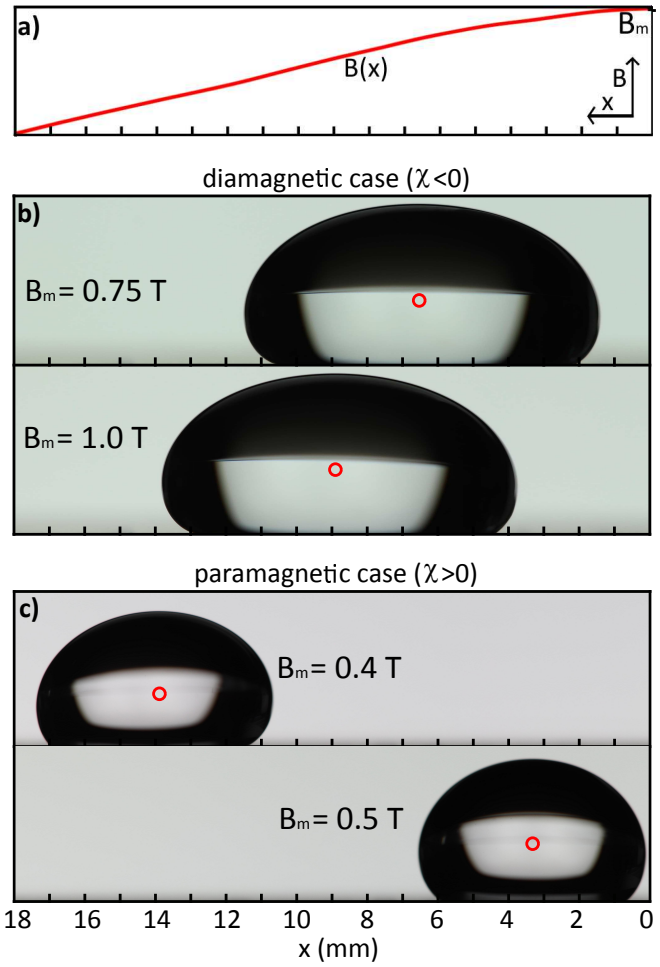

FIG. 3. Transport of dia- and paramagnetic drops in a non-uniform magnetic field. (a) Illustration of the profile of the magnetic field, which decays along the x-axis from its maximum value B_m. As B_m is increased, a 300 μl drop of sodium sulphate solution is pushed away from the region of highest field strength (b), while a 100 μl of manganese chloride is pulled towards the region of highest field strength (c). The positions of the centre-of-masses are indicated as red circles. The properties of the salt solutions are summarized in Table II.

IV. SUMMARY AND CONCLUSION

In summary, we have used the EMST to describe the shape of diamagnetic drops in magnetic fields. We found a shortening of the drops along the direction of magnetic field lines, which stands in contrast to the elongation along the field lines of drops with a positive magnetic susceptibility, such as paramagnetic or ferrofluidic drops. The strength of the deformation scales with the total magnetic moment induced in the drop, which is proportional to the volume and magnetic susceptibility of the drop. We demonstrated that diamagnetic drops in non-uniform magnetic fields are transported away from the region of highest magnetic field strength. This stands in contrast to the transport of paramagnetic drops, which is directed towards the region of highest magnetic field strength. Though the presented solutions have a too high osmolality to contain mammalian cells (2 osm/kg and 8 osm/kg for the sodium sulphate and calcium bromide solutions respectively), further dilution and usage of stronger magnetic fields may permit suspension and transport of mammalian or plant cells. This technique may also be applied to suspension and transport of DNA or other macromolecules such as proteins.

In conclusion, our work demonstrates that the EMST captures the magnetic forces acting on fluids due to magnetostatic fields and electrostatic fields. This tool aids the study of bulk diamagnetism and our findings highlight the natural place of diamagnetic fluids amongst the tools of microfluidics and DMF.

ACKNOWLEDGMENTS

The work by JD has been funded by the Engineering and Physical Sciences Research Council (EPSRC): EP/L016753/1.

[1] G. M. Whitesides, Nature **442**, 368 (2006).
[2] S.-Y. Teh, R. Lin, L.-H. Hung, and A. P. Lee, Lab on a Chip **8**, 198 (2008).
[3] R. Seemann, M. Brinkmann, T. Pfohl, and S. Herminghaus, Reports on Progress in Physics **75**, 016601 (2012).
[4] K. Choi, A. H. Ng, R. Fobel, and A. R. Wheeler, Annual Review of Analytical Chemistry **5**, 413 (2012).
[5] E. M. Miller and A. R. Wheeler, Analytical and Bioanalytical Chemistry **393**, 419 (2009).
[6] M. J. Jebrail and A. R. Wheeler, Current Opinion in Chemical Biology **14**, 574 (2010).
[7] S. L. S. Freire, Sensors and Actuators, A: Physical **250**, 15 (2016).
[8] M. G. Lippmann, Annales de Chimie et de Physique, 5 serie, t. V (1875).
[9] H. Pellat, Comptes rendus hebdomadaires des séances de l ' Académie des sciences, Série B **123**, 123 (1896).
[10] B. Berge, Comptes Rendus de L'Academie des Sciences Paris, Serie, II **317**, 157 (1993).
[11] S. K. Cho, H. Moon, and C. J. Kim, Journal of Microelectromechanical Systems **12**, 70 (2003).
[12] F. Mugele and J.-C. Baret, Journal of Physics: Condensed Matter **17**, R705 (2005).
[13] W. C. Nelson and C. J. C. Kim, Journal of Adhesion Science and Technology **26**, 1747 (2012).
[14] T. B. Jones, Journal of Electrostatics **51-52**, 290 (2001).
[15] P. R. Gascoyne, J. V. Vykoukal, J. A. Schwartz, T. J. Anderson, D. M. Vykoukal, K. W. Current, C. McConaghy, F. F. Becker, and C. Andrews, Lab on a Chip **4**, 299 (2004).
[16] G. McHale, C. V. Brown, M. I. Newton, G. G. Wells, and N. Sampara, Physical Review Letters **107**, 186101 (2011).
[17] H. Geng, J. Feng, L. M. Stabryla, and S. K. Cho, Lab on a Chip **17**, 1060 (2017).
[18] R. Pethig, Journal of The Electrochemical Society **164**, 3049 (2017).
[19] M. P. Hughes, Biomicrofluidics **10** (2016), 10.1063/1.4954841.
[20] H. A. Pohl and I. Hawk, Science **152**, 647 (1966).
[21] N. Pamme, Lab Chip **6**, 24 (2006).
[22] Y. Zhang and N.-T. Nguyen, Lab Chip **17**, 994 (2017).
[23] M. Latikka, M. Backholm, J. V. Timonen, and R. H. Ras, Current Opinion in Colloid and Interface Science **36**, 118 (2018).
[24] O. E. Séro-Guillaume, D. Zouaoui, D. Bernardin, and J. P. Brancher, Journal of Fluid Mechanics **241**, 215 (1992).
[25] S. Afkhami, A. J. Tyler, Y. Renardy, M. Renardy, T. G. St. Pierre, R. C. Woodward, and J. S. Riffle, Journal of Fluid Mechanics **663**, 358 (2010).
[26] P. Rowghanian, C. D. Meinhart, and O. Campàs, Journal of Fluid Mechanics **802**, 245 (2016).
[27] A. Egatz-Gómez, S. Melle, A. A. García, S. A. Lindsay, M. Márquez, P. Domínguez-García, M. A. Rubio, S. T. Picraux, J. L. Taraci, T. Clement,

D. Yang, M. A. Hayes, and D. Gust, Applied Physics Letters **89**, 034106 (2006).
[28]L. Mats, R. Young, G. T. T. Gibson, and R. D. Oleschuk, Sensors and Actuators, B: Chemical **220**, 5 (2015).
[29]J. Dodoo, G. McHale, and A. A. Stokes, (2019), arXiv:1908.05193.
[30]E. Bormashenko, Advances in Colloid and Interface Science **269**, 1 (2019).
[31]D. Laumann, The Physics Teacher **56**, 352 (2018).
[32]M. Frenkel, V. Danchuk, V. Multanen, I. Legchenkova, Y. Bormashenko, O. Gendelman, and E. Bormashenko, Langmuir **34**, 6388 (2018).
[33]O. Gendelman, M. Frenkel, V. Fliagin, N. Ivanova, V. Danchuk, I. Legchenkova, A. Vilk, and E. Bormashenko, Surface Innovations **7**, 194 (2019).
[34]F. Sauer and R. Schlogel, in *Interactions between electromagnetic fields and cells*, edited by A. Chiabrera, C. Nicolini, and H. P. Schwan (Plenum Publishing Corporation, 1985) pp. 203–251.
[35]T. B. Jones, Langmuir **18**, 4437 (2002).
[36]X. Wang, X.-B. Wang, and P. R. Gascoyne, Journal of Electrostatics **39**, 277 (1997).
[37]T. B. Jones, K. L. Wang, and D. J. Yao, Langmuir **20**, 2813 (2004).
[38]J. C. Bacri and D. Salin, Journal de Physique Lettres **43**, 649 (1982).
[39]H. A. Stone, J. R. Lister, and M. P. Brenner, Proceedings of the Royal Society A: Mathematical, Physical and Engineering Sciences **455**, 329 (1999).
[40]K. Stierstadt and M. Liu, ZAMM Zeitschrift fur Angewandte Mathematik und Mechanik **95**, 4 (2015).
[41]C. A. Miller and P. Neogi, *Interfacial phenomena : equilibrium and dynamic effects*, 2nd ed., Surfactant science series ; v. 139 (CRC Press, London, 2008) pp. 1–29.
[42]V. A. Lubarda and K. A. Talke, Langmuir **27**, 10705 (2011).
[43]A. W. Adamson, *Physical chemistry of surfaces*, 5th ed. (New York : John Wiley & Sons, Inc., New York, 1990).
[44]G. I. Taylor, Proceedings of the Royal Society of London. Series A, Mathematical and Physical Sciences **291**, 159 (1966).
[45]J. R. Melcher and G. I. Taylor, Annual Review of Fluid Mechanics **1**, 111 (1969).
[46]J. D. Sherwood, Journal of Fluid Mechanics **188**, 133 (1988).
[47]L. T. Corson, C. Tsakonas, B. R. Duffy, N. J. Mottram, I. C. Sage, C. V. Brown, and S. K. Wilson, Physics of Fluids **26**, 1 (2014).
[48]J. R. Rumble, in *CRC Handbook of Chemistry and Physics, 99th Edition (Internet Version 2018)* (CRC Press/Taylor & Francis, Boca Raton, FL).
[49]I. S. Bayer, V. Caramia, D. Fragouli, F. Spano, R. Cingolani, and A. Athanassiou, Journal of Materials Chemistry **22**, 2057 (2012).
[50]G. P. Zhu, N. T. Nguyen, R. V. Ramanujan, and X. Y. Huang, Langmuir **27**, 14834 (2011).